

NANO EXPRESS

Open Access



Electronic Structure and I - V Characteristics of InSe Nanoribbons

A-Long Yao¹, Xue-Feng Wang^{1,2*} , Yu-Shen Liu^{3*} and Ya-Na Sun¹

Abstract

We have studied the electronic structure and the current-voltage (I - V) characteristics of one-dimensional InSe nanoribbons using the density functional theory combined with the nonequilibrium Green's function method. Nanoribbons having bare or H-passivated edges of types zigzag (Z), Klein (K), and armchair (A) are taken into account. Edge states are found to play an important role in determining their electronic properties. Edges Z and K are usually metallic in wide nanoribbons as well as their hydrogenated counterparts. Transition from semiconductor to metal is observed in hydrogenated nanoribbons HZZH as their width increases, due to the strong width dependence of energy difference between left and right edge states. Nevertheless, electronic structures of other nanoribbons vary with the width in a very limited scale. The I - V characteristics of bare nanoribbons ZZ and KK show strong negative differential resistance, due to spatial mismatch of wave functions in energy bands around the Fermi energy. Spin polarization in these nanoribbons is also predicted. In contrast, bare nanoribbons AA and their hydrogenated counterparts HAAH are semiconductors. The band gaps of nanoribbons AA (HAAH) are narrower (wider) than that of two-dimensional InSe monolayer and increase (decrease) with the nanoribbon width.

Keywords: InSe monolayer nanoribbon, Electronic structure, Negative differential resistance, Semiconductor-metal transition

Background

Atomically thin two-dimensional (2D) materials have attracted intensive interest in the last decade due to their unique electronic properties and promising application potential [1–4] mainly originated from their reduced dimensionality. One-dimensional (1D) nanoribbons can then be fabricated by tailoring the 2D materials [5] or assembling atoms precisely in the bottom-up way [6, 7]. In the nanoribbons, the electronic properties are further modulated by additional confinement and possible edge functionalization [8, 9]. For example, their energy gap, a key parameter of semiconductor, may be continuously adjusted by their width [10–15]. The dangling bonds of the edge atoms can be passivated by H atoms in proper environment, and the hydrogenation may stabilize the edges from structural reconstruction [16, 17].

Recently, a new member, the InSe monolayer, has been added to the 2D materials. Bulk InSe belongs to the family of layered metal chalcogenide semiconductors and has been intensively studied in the last decades [18–22]. Each of its quadruple layers has a hexagonal lattice that effectively consists of four covalently bonded Se–In–In–Se atomic planes. The quadruple layers are stacked together by van der Waals interactions at an interlayer distance around 0.8 nm. The stacking style defines its polytypes such as β , γ , and ϵ , among which the β and γ ones have direct band gaps. Nevertheless, the single quadruple InSe layer was successfully fabricated only in the last years by the mechanical exfoliation method [23, 24]. Since then, the observed extraordinary high electron mobility and special physical properties of InSe monolayers have triggered extensive study on their possible applications in optoelectronic devices [24–26] and electronic devices [27, 28]. For the sake of exploring novel functional properties, theoretical study can also be an efficient approach. Numerical simulations of structural, electric, and magnetic properties of InSe monolayers and their

* Correspondence: wxf@suda.edu.cn; yslu@cslg.edu.cn

¹Jiangsu Key Laboratory of Thin Films, College of Physics, Optoelectronics and Energy, Soochow University, 1 Shizi Street, Suzhou 215006, China

³College of Physics and Engineering, Changshu Institute of Technology, Changshu 215500, China

Full list of author information is available at the end of the article

modulation by doping, defect, and, adsorption have been carried out [29–38]. The band structures of mono- and few-layer InSe have been carefully studied by density functional theory [29]. The dominant intrinsic defects in InSe monolayer have been figured out [30], and the properties of native defects and substitutional impurities in monolayer InSe have been estimated by calculation of formation and ionization energies [31]. In addition, it has been predicted that substitutional doping of As atoms can transfer InSe monolayer from nonmagnetic semiconductor to magnetic semiconductor/metal or half-semimetal [32]. The thermal conductivity of InSe monolayers can be greatly modulated by their size [33]. However, to our best knowledge, there are few studies on electronic properties of one-dimensional nanoribbons of InSe monolayer up to now.

In this paper, we carry out first-principles simulation on electronic properties of 1D bare zigzag, armchair, and Klein monolayer InSe nanoribbons and their hydrogen-passivated counterparts. Our studies indicate the transition from semiconductor to metal in hydrogen-passivated InSe zigzag nanoribbons and the interesting energy gap change in armchair nanoribbons. The current-voltage curves show diversified electric properties for nanoribbons with different edges.

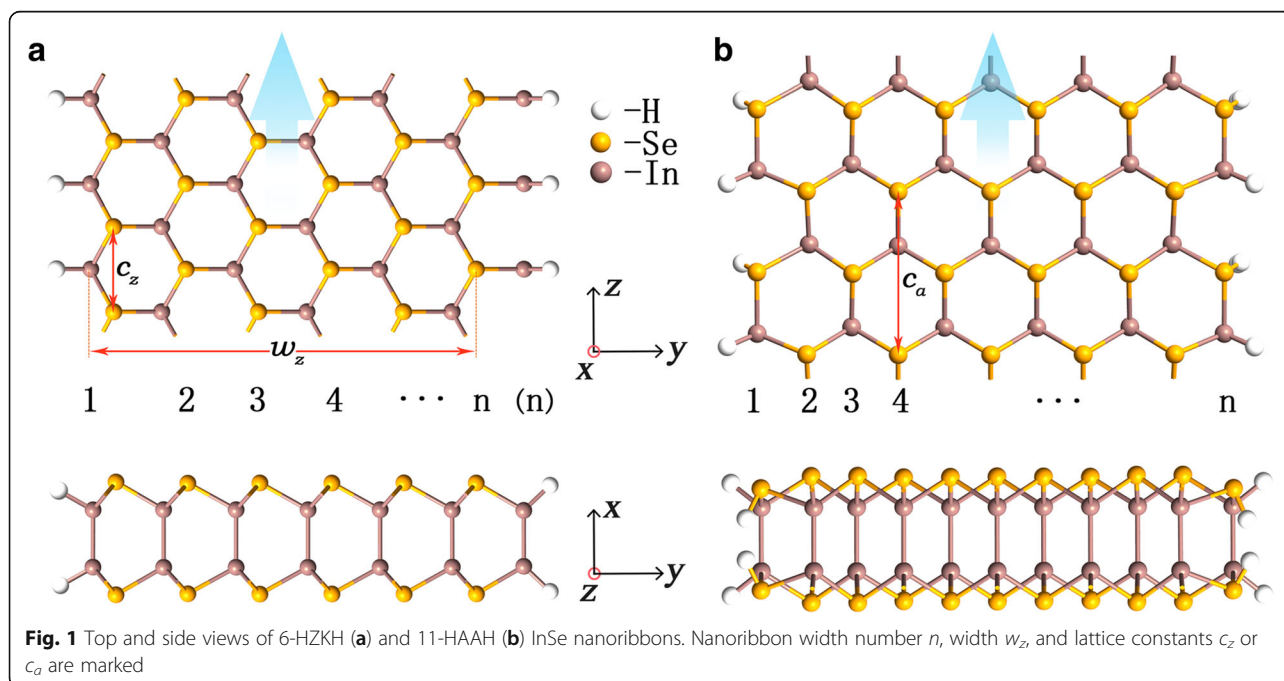
Methods

The three typical edge patterns of honeycomb lattice, zigzag (Z), armchair (A), and Klein (K) are taken into account [39]. As illustrated in Fig. 1, a nanoribbon can be identified by its width number n and the combination of

the types of its two edges. There are five classes of bare nanoribbons: n -ZZ, n -AA, n -KK, n -ZK, and n -KZ. Note that n -ZK is different from n -KZ because we assume that the left (right) Z edge ends with In (Se) atoms. If each edge atom is passivated by one hydrogen atom, we denote the passivated nanoribbons as n -HZZH, n -HAAH, n -HKKH, n -HZKH, and n -HKZH, respectively. A Se-In-In-Se quadruple layer of lattice constant 4.05 Å with Se-In layer distance 0.055 Å and In-In layer distance 0.186 Å is used to make nanoribbons before geometry optimization [21].

All the computations are performed using the Atomistix ToolKit (ATK) based on DFT with the pseudopotential technique. The exchange correlation functional in the local spin density approximation with the Perdew–Zunger parameterization (LSDA-PZ) is adopted. The wave functions are expanded on a basis set of double- ζ orbitals plus one polarization orbital (DZP). An energy cutoff of 3000 eV, a k -space mesh grid of $1 \times 1 \times 100$, and an electronic temperature of 300 K are used in the real-axis integration for the non-equilibrium Green's functions. A 15-Å thick vacuum layer in the supercells is adopted to separate the nanoribbons from their neighbor images in both x and y directions and to ensure the suppression of the coupling between them. Band structures are calculated after full geometry relaxation with a force tolerance of 0.02 eV/\AA^{-1} .

To simulate the electronic transport property of the nanoribbons, we connect each one into a circuit with left (right) chemical potential $\mu_L(\mu_R)$ [40, 41]. The nanoribbon can then be partitioned into three regions, the left



(right) electrode L (R) and the central region C. The spin-dependent current can be estimated by the Landauer-Büttiker formula [42].

$$I_{\sigma}(V_b) = \frac{e}{h} \int_{-\infty}^{+\infty} T_{\sigma}(E, V_b) [f_L(E - \mu_L) - f_R(E - \mu_R)] dE$$

with spin $\sigma = \uparrow, \downarrow$ and voltage bias $V_b = (\mu_R - \mu_L)/e$. Here, $T_{\sigma}(E, V_b) = \text{Tr}[\Gamma_L G_{\sigma} \Gamma_R G_{\sigma}^{\dagger}]$ is the transmission spectrum with G_{σ} the retarded Green's function in region C and Γ_L (Γ_R) the coupling matrix between C and L (R). f_L (f_R) is the Fermi distribution function of electrons in L (R).

Results and Discussion

In Fig. 1, we scheme the top and side views of (a) 6-HZKH and (b) 11-HAAH nanoribbons with lattice constants $c_z = 4.05 \text{ \AA}$ and $c_a = 7.01 \text{ \AA}$, respectively. Edge K is along the direction parallel to that of edge Z. The extending direction z of the nanoribbon is marked by blue arrows. Different from the case in graphene nanoribbon [39], no edge reconstruction is observed for the three edge styles in both bare and H-passivated InSe nanoribbons, and our simulation indicates that they are all energetically stable.

Bare n -ZZ nanoribbons are magnetic metal except the 2-ZZ one which has a reconstructed geometry and appears semiconductor. They have similar band structures as illustrated in Fig. 2a. The p orbitals of edge Se atoms dominate the contribution to the states near the Fermi energy similar to the case of InSe monolayer [32], but more contributions from the In atoms are observed

here. The two partially occupied bands are from the left and right edge states, respectively, as shown by the Γ -point Bloch states for 4-ZZ nanoribbon. One of them is spin split and a net magnetic moment, e.g., $0.706 \mu_B$ for 4-ZZ nanoribbon, appears in each primitive cell on the left edge.

When the edge atoms are passivated by H atoms, n -HZZH nanoribbons become nonmagnetic semiconductor for $n = 3, 4$ and metal for $n > 4$ as shown in Fig. 2b. Note that the structure becomes unstable for $n = 2$. In 4-HZZH nanoribbon, the Bloch states at Γ in conduction (valence) bands near the Fermi energy are confined to the right (left) edge. They have components similar to those in 2D InSe monolayer except the H atomic orbital parts. The highest five bands of the left edge states are composed of one p_x , two p_y , and two p_z orbitals of Se edge atoms. The energy bands of the right (left) edge states are similar to the conduction (valence) bands in the Γ -K direction of 2D InSe monolayer [32]. Their separation in energy depends strongly on n though their dispersions are insensitive to n . We define E_d as the energy difference between the minimum of the right edge states and maximum of the left edge states.

In Fig. 3, we plot E_d versus n and w_z and found approximately an inverse dependence $E_d \approx E_0 + a/(w_z - w_0)$ with $E_0 = -0.45 \text{ eV}$, $w_0 = 4 \text{ \AA}$, and $a = 4 \text{ eV \AA}$. This behavior is similar to the width dependence of energy gap in zigzag graphene and B-N nanoribbons [12–15, 43–47] having origin of electron-electron interaction. Narrow HZZH InSe nanoribbons are semiconductors, and a transition from semiconductor to metal occurs as the width increases.

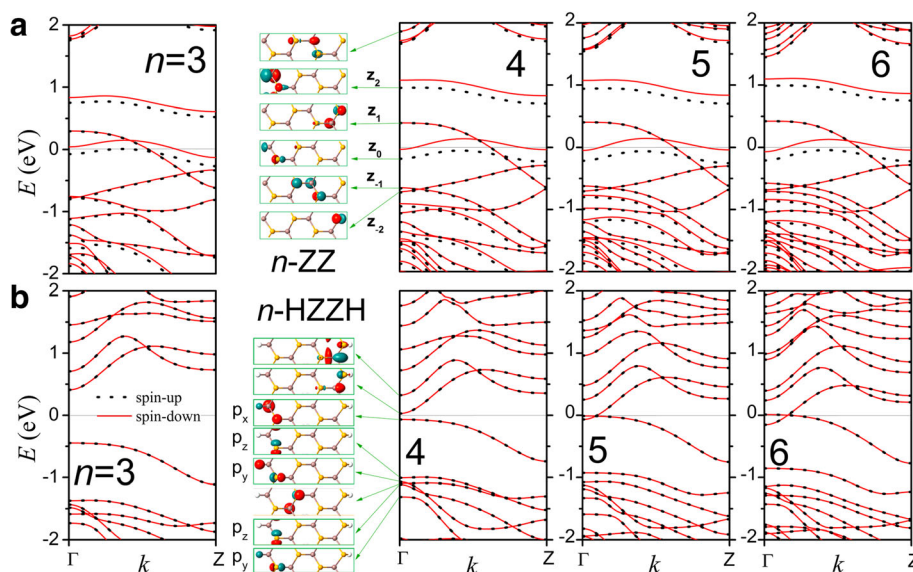
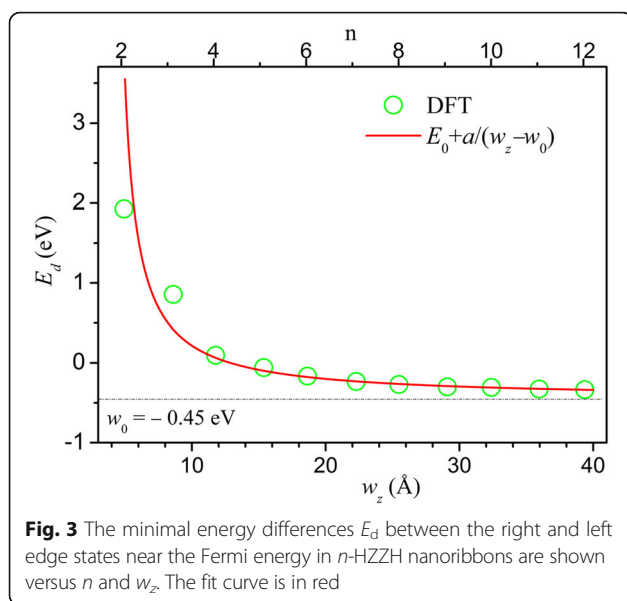


Fig. 2 The band structures of **a** 3-, 4-, 5-, and 6-ZZ nanoribbons and **b** 3-, 4-, 5-, and 6-HZZH nanoribbons. Γ -point Bloch states near the Fermi energy are shown for $n = 4$. The orbits of the states below the Fermi energy are indicated for 4-HZZH nanoribbon

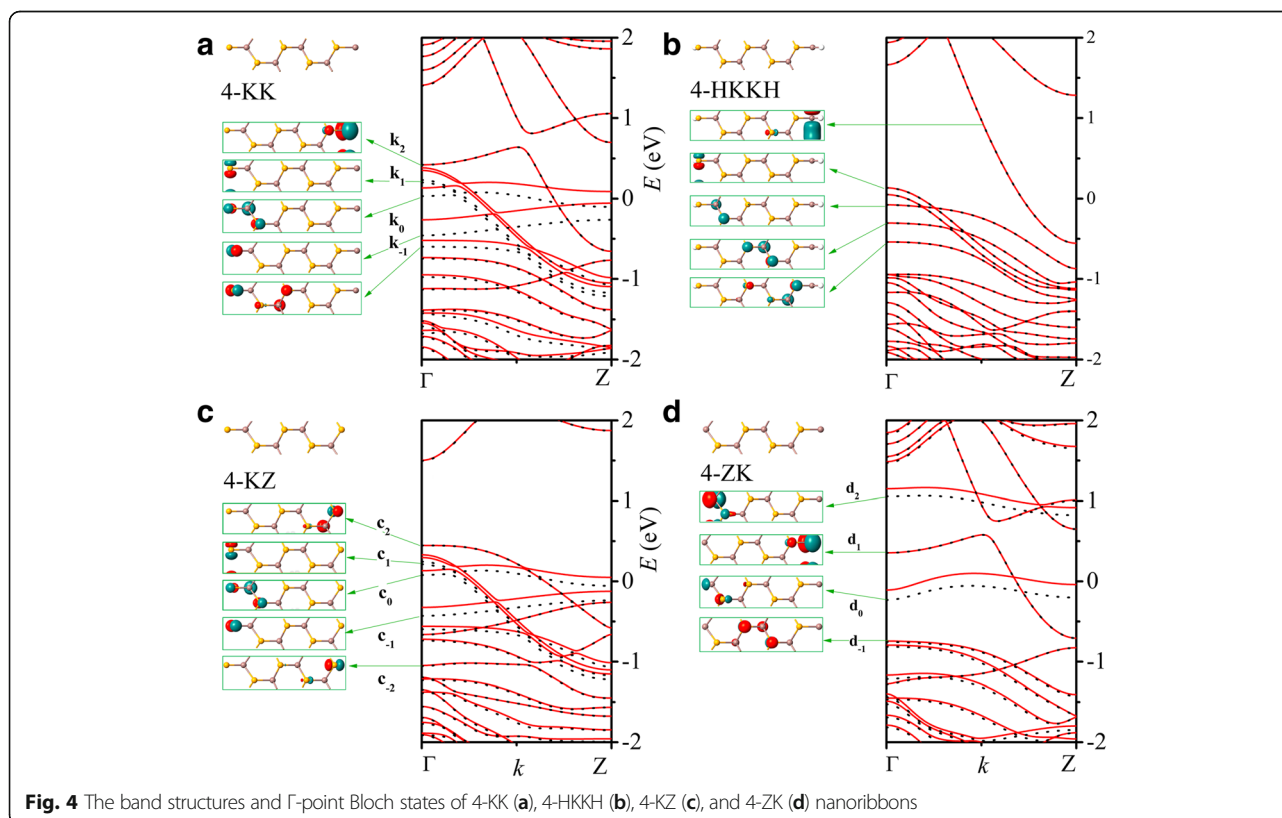


The band structures of n -KK and n -HKKH nanoribbons are not sensitive to the width number n as exemplified in Fig. 4a, b, respectively, for $n = 4$. Compared to zigzag edge, bare Klein edge has more dangling bonds which results in significant change of the band structure. Orbitals of edge Se atoms usually have lower energy than those of edge In atoms, similar to ZZ nanoribbon.

In HKKH nanoribbons, the suppression of the p orbital of edge In atoms and the p orbital of edge Se atom by the passivation of H atoms is obvious. Nevertheless, one H atom is not enough to passivate all the dangling bonds of the edge atoms. Both KK and HKKH nanoribbons are metal.

In nanoribbons with a mixing of zigzag and Klein edges, we observe a combination of energy bands of the two kinds of edges near the Fermi energy. As shown in Fig. 4c for the 4-KZ nanoribbon, the dispersion and Γ -point Bloch states of bands c_1 , c_0 , and c_{-1} are the same as those of band k_1 , k_0 , and k_{-1} in 4-KK nanoribbon as plotted in Fig. 4a, while bands c_2 and c_{-2} are the same as band z_1 and z_{-2} of 4-ZZ nanoribbons in Fig. 2a. Similarly, the band structure of the 4-ZK nanoribbon, as illustrated in Fig. 4d, is composed of band d_1 from the right Klein edge and bands d_2 , d_0 , and d_{-1} from the left zigzag edge. Since n -ZK and n -KZ nanoribbons keep part of the energy bands of n -KK nanoribbons near the Fermi energy, they are both metal as the n -KK nanoribbons. For the same reason, the H-passivated nanoribbons mixing edges Z and K are also metallic.

Both the AA and HAAH nanoribbons are nonmagnetic semiconductors as shown in Fig. 5a, b, where the band structures are plotted for $n = 4, 5$. The passivation of H atoms can improve the structural stability energetically and enlarges the energy gap. Interestingly, the energy gap



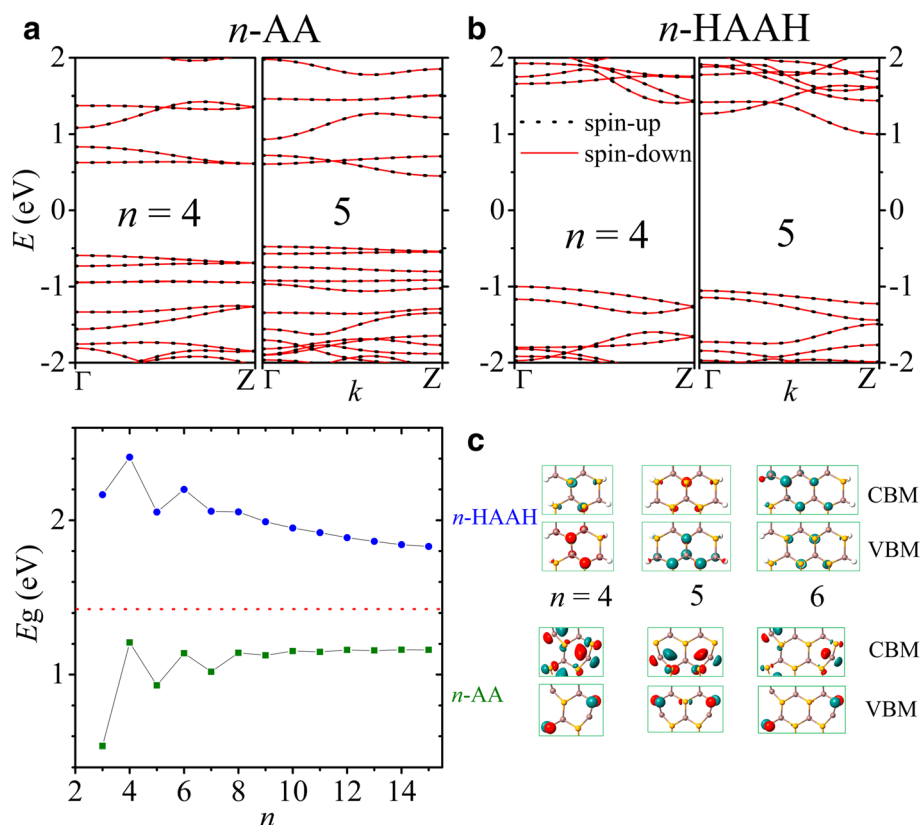


Fig. 5 The band structures of 4- and 5-AA nanoribbons are shown in **a** and those of 4- and 5-HAAH in **b**. The energy gaps E_g of n -AA (green) and n -HAAH (blue) nanoribbons are plotted versus n in **c** with the gap of InSe monolayer (red) marked. The Bloch states at CBM and VBM for $n = 4, 5$, and 6 are shown in the right panels of **c**

has a zigzag dependence on the nanoribbon width, showing an odd-even family-like behavior as in graphene and B-N nanoribbons [10–15, 43–47]. As illustrated in Fig. 5c, n -AA nanoribbons have a gap (olive square) narrower than that of 2D InSe monolayer (red dash). The gap increases (decreases) monotonically with the width for odd (even) n and converges to a value of 1.15 eV at the large width limit when the two edges are decoupled from each other and stable their energy [13]. The Bloch states of valence band maximum (VBM) at Γ point and conduction band minimum (CBM) at Z point are also shown in Fig. 5c. The parity behavior is observed again with the symmetric ($n=5$) or diagonal ($n=4, 6$) distribution of the states around edge Se atoms at VBM and around edge In atoms at CBM.

On the other hand, the gaps of n -HAAH nanoribbons (blue circle) are wider than their 2D counterpart and decrease with the width for both odd and even n . In passivated nanoribbons, the Bloch states at VBM and CBM have much less edge component. The corresponding energy gaps are about 1 eV wider than those of the bare nanoribbons, and the difference diminishes with width increase [13].

In Fig. 6a, we show the current-voltage (I - V) characteristic of above metallic InSe nanoribbons 4-ZZ (square), 4-KK (circle), and 4-HKKH (triangle). Spin-up (spin-down) curves are marked by filled (empty) symbols. The Landauer-Büttiker formula has been employed to calculate the spin dependent current I_σ when a voltage bias V_b is applied between electrodes L and R, with $\mu_R = eV_b/2$ and $\mu_L = -eV_b/2$ assumed. Negative differential resistance (NDR) and spin polarization are observed in 4-ZZ and 4-KK bare nanoribbons under a bias in the region between 0.5 and 1.2 V. The peak-to-valley ratio of NDR is larger than 10 for the 4-ZZ nanoribbon due to the transversal mismatch of wave functions among energy bands near the Fermi energy as illustrated in Fig. 2a and explained in the following. Band z_1 is the dominant transport channel under $V_b < 1.2$ V as indicated by the spin-up and spin-down transmission spectra in Fig. 6b, c, respectively. However, the wave functions of band z_1 are orthogonal to or are separated in space from those of nearby bands z_2 , z_{-1} , and z_{-2} . This leads to the mismatch between the states z_1 in one electrode and those of the same energy in the other electrode under V_b . The

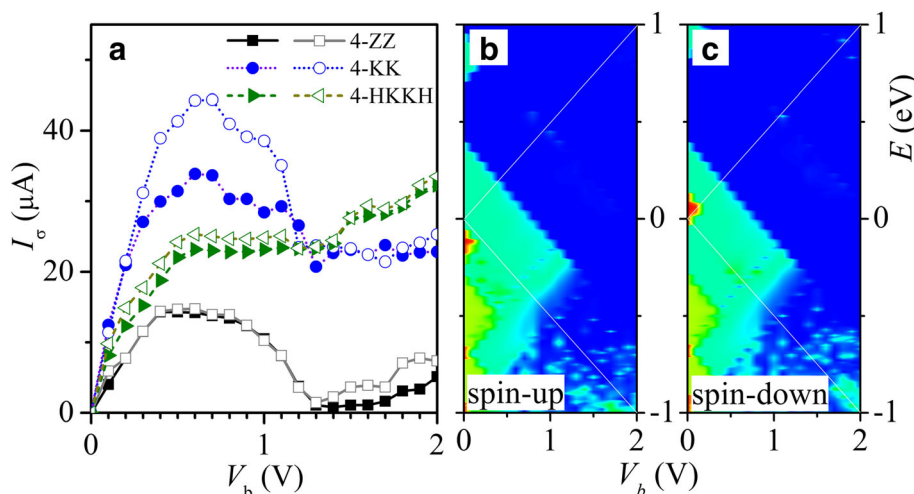


Fig. 6 **a** The spin-up (filled) and spin-down (empty) I - V characteristics of 4-ZZ (square), 4-KK (circle), and 4-HKKH (triangle) InSe nanoribbons are presented. The corresponding transmission spectra of spin-up (**b**) and spin-down (**c**) are shown for the 4-ZZ nanoribbon. The transport window between μ_L and μ_R is marked by the white lines

electrons from band z_1 in one electrode then have difficulty to transport to the other electrode with energy conservation. As a result, the I - V curve of nanoribbon 4-ZZ shows a single-band characteristic with strong NDR. Furthermore, the spin split of band z_0 leads to the spin polarization in the linear regime. In the passivated 4-HKKH nanoribbon, however, the current saturates in the above NDR bias region.

Conclusions

We have systematically investigated the electronic properties of InSe nanoribbons with Z, A, or K edges. The edges play a key role in determining the properties since electron states near the Fermi energy have big weight of edge atomic orbitals. Bare Z and K edges are conductive and magnetic. Strong edge-edge interaction may lead to the transition of n -HZZH nanoribbons from semiconductor to metal as n increases. As a result, bare and H-passivated nanoribbons with Z and K edges are metallic except very narrow ones. n -AA and n -HAAH are non-magnetic semiconductors with energy gaps narrower and wider, respectively, than that of InSe monolayer. Their gaps approach each other in a zigzagged way as n increases, showing an even-odd behavior. The current-voltage curves of ZZ and KK nanoribbons are characterized by strong single-band NDR and spin polarization.

Abbreviations

1D: One-dimensional; 2D: Two-dimensional; A: Armchair; CBM: Conduction band minimum; K: Klein; VBM: Valence band maximum; Z: Zigzag

Funding

This work was supported by the National Natural Science Foundation of China (grant nos. 61674110, 61674022, and 91121021).

Availability of Data and Materials

The datasets supporting the conclusions of this article are included within the article.

Authors' Contributions

XFW conceived the research work. ALY and YNS carried out the computation. ALY, XFW, and YSL analyzed the results and wrote the manuscript. All the authors read and approved the final manuscript.

Authors' Information

XFW is a professor in the College of Physics, Optoelectronics and Energy, Soochow University. He obtained his BSc degree in 1989 from Shanghai Jiaotong University and earned his PhD degree in 1994 at Shanghai Institute of Microsystem and Information Technology, Chinese Academy of Science. YSL is a professor in the College of Physics and Engineering, Changshu Institute of Technology.

Competing Interests

The authors declare that they have no competing interests.

Publisher's Note

Springer Nature remains neutral with regard to jurisdictional claims in published maps and institutional affiliations.

Author details

¹Jiangsu Key Laboratory of Thin Films, College of Physics, Optoelectronics and Energy, Soochow University, 1 Shizi Street, Suzhou 215006, China. ²Key Laboratory of Terahertz Solid-State Technology, Chinese Academy of Sciences, 865 Changning Road, Shanghai 200050, China. ³College of Physics and Engineering, Changshu Institute of Technology, Changshu 215500, China.

Received: 5 February 2018 Accepted: 5 April 2018

Published online: 18 April 2018

References

1. Castro Neto AH, Guinea F, Peres NMR, Novoselov KS, Geim AK (2009) The electronic properties of graphene. *Rev Mod Phys* 81:109–162
2. Abergel D, Apalkov V, Berashevich J, Ziegler K, Chakraborty T (2010) Properties of graphene: a theoretical perspective. *Adv Phys* 59:261–482
3. Feng YP, Shen L, Yang M, Wang AZ, Zeng MG, Wu QY, Chintalapati S, Chang CR (2017) Prospects of spintronics based on 2D materials. *WIREs Comput Mol Sci* 7:e1313

4. Tan CL, Cao XD, Wu XJ, He QY, Yang J, Zhang X, Chen JZ, Zhao W, Han SK, Nam GH, Sindoro M, Zhang H (2017) Recent advances in ultrathin two-dimensional nanomaterials. *Chem Rev* 117(9):6225–6331
5. Wang XR, Ouyang YJ, Li XL, Wang HL, Guo J, Dai HJ (2008) Room-temperature all-semiconducting sub-10-nm graphene nanoribbon field-effect transistors. *Phys Rev Lett* 100:206803
6. Cai JM, Ruffieux P, Jaafar R, Bieri M, Braun T, Blankenburg S, Muoth M, Seitsonen AP, Saleh M, Feng XL, Mullen K, Fasel R (2010) Atomically precise bottom-up fabrication of graphene nanoribbons. *Nature* 466:470–473
7. Ruffieux P, Wang SY, Yang B, Sanchez CS, Liu J, Dienel T, Talirz L, Shinde P, Pignedoli CA, Passerone D, Dumsclaff T, Feng XL, Mullen K, Fasel R (2016) On-surface synthesis of graphene nanoribbons with zigzag edge topology. *Nature* 531:489–492
8. Chen C, Wang XF, Li YS, Cheng XM, Yao AL (2017) Single-band negative differential resistance in metallic armchair MoS_2 nanoribbons. *J Phys D* 50: 465302
9. Zhai MX, Wang XF (2016) Atomistic switch of giant magnetoresistance and spin thermopower in graphene-like nanoribbons. *Sci Rep* 6:36762
10. Li YF, Zhou Z, Zhang SB, Chen ZF (2008) MoS_2 nanoribbons: high stability and unusual electronic and magnetic properties. *J Am Chem Soc* 130: 16739–16744
11. Ataca C, Sahin H, Akturk E, Ciraci S (2011) Mechanical and electronic properties of MoS_2 nanoribbons and their defects. *J Phys Chem C* 115: 3934–3941
12. Du AJ, Smith SC, Lu GQ (2007) First-principle studies of electronic structure and C-doping effect in boron nitride nanoribbon. *Chem Phys Lett* 447:181–186
13. Park CH, Louie SG (2008) Energy gaps and stark effect in boron nitride nanoribbons. *Nano Lett* 8:2200–2203
14. Nakamura J, Nitta T, Natori A (2005) Electronic and magnetic properties of BNC ribbons. *Phys Rev B* 72:205429
15. Son YW, Cohen ML, Louie SG (2006) Energy gaps in graphene nanoribbons. *Phys Rev Lett* 97:216803
16. Datta SS, Strachan DR, Khamis SM, Johnson ATC (2008) Crystallographic etching of few-layer graphene. *Nano Lett* 8:1912–1915
17. Zhang XW, Yazayev OV, Feng JJ, Xie LM, Tao CG, Chen YC, Jiao LY, Pedramrazi Z, Zettl A, Louie SG, Dai HJ, Crommie MF (2013) Experimentally engineering the edge termination of graphene nanoribbons. *ACS Nano* 7(1):198–202
18. Gomes da Costa P, Dandrea RG, Wallis RF, Balkanski M (1993) First-principles study of the electronic structure of γ -InSe and β -InSe. *Phys Rev B* 48:14135
19. Camara MOD, Mauger A, Devos I (2002) Electronic structure of the layer compounds GaSe and InSe in a tight-binding approach. *Phys Rev B* 65:125206
20. Ma YD, Dai Y, Yu L, Niu CW, Huang BB (2013) Engineering a topological phase transition in β -InSe via strain. *New J Phys* 15:073008
21. Han G, Chen ZG, Drennan J, Zou J (2014) Indium selenides: structural characteristics, synthesis and their thermoelectric performances. *Small* 14:2747
22. Rybkovskiy DV, Osadchy AV, Obraztsova ED (2014) Transition from parabolic to ring-shaped valence band maximum in few-layer GaS, GaSe, and InSe. *Phys Rev B* 90:235302
23. Bandurin DA, Tyurnina AV, Yu GL, Mishchenko A, Viktor Z, Morozov SV, Kumar RK, Gorbachev RV, Kudrynskiy ZR, Sergio P, Kovalyuk ZD, Zeitler U, Novoselov KS, Patane A, Eaves L, Grigorieva IV, Falko VI, Geim AK, Cao Y (2016) High electron mobility, quantum Hall effect and anomalous optical response in atomically thin InSe. *Nat Nanotechnol* 12:223–227
24. Lei SD, Ge LH, Najmaei S, George A, Kappera R, Lou J, Chhowalla M, Yamaguchi H, Gupta G, Vajtai R, Mohite AD, Ajayan PM (2014) Evolution of the electronic band structure and efficient photo-detection in atomic layers of InSe. *ACS Nano* 8(2):1263–1272
25. Lei SD, Wen FF, Li B, Wang QZ, Huang YH, He YM, Dong P, Bellah J, George A, Ge LH, Lou J, Halas NJ, Vajtai R, Ajayan PM (2015) Optoelectronic memory using two dimensional materials. *Nano Lett* 15:259–265
26. Tamalampudi SR, Lu YY, Kumar RU, Sankar R, Liao CD, Moorthy BK, Cheng CH, Chou FC, Chen YT (2014) High performance and bendable few-layered InSe photodetectors with broad spectral response. *Nano Lett* 14(5):2800–2806
27. Sucharitakul S, Goble NJ, Kumar UR, Sankar R, Bogorad ZA, Chou FC, Chen YT, Gao XPA (2015) Intrinsic electron mobility exceeding $10^3 \text{ cm}^2/(\text{V s})$ in multilayer InSe FETs. *Nano Lett* 15(6):3815–3819
28. Feng W, Zheng W, Cao WW, Hu PA (2014) Back gated multilayer InSe transistors with enhanced carrier mobilities via the suppression of carrier scattering from a dielectric interface. *Adv Mater* 26:6587–6593
29. Guo YZ, Robertson J (2017) Band structure, band offsets, substitutional doping, and Schottky barriers of bulk and monolayer InSe. *Phys Rev Mater* 1:044004
30. Xiao KJ, Carvalho A, Neto AHC (2017) Defects and oxidation resilience in InSe. *Phys Rev B* 96:054112
31. Wang D, Li XB, Sun HB (2017) Native defects and substitutional impurities in two-dimensional monolayer InSe. *Nano* 9:11619–11624
32. Sun YN, Wang XF, Zhai MX, Yao AL (2017) Tunable magnetism and metallicity in As-doped InSe quadruple layers. *J Phys D* 50:215003
33. Nissimagoudar AS, Ma JL, Chen YN, Li W (2017) Thermal transport in monolayer InSe. *J Phys Condens Matter* 29:335702
34. Ma DW, Ju WW, Tang YA, Chen Y (2017) First-principles study of the small molecule adsorption on the InSe monolayer. *Appl Surf Sci* 426:244–252
35. Li XP, Xia CX, Song XH, Du J, Xiong WQ (2017) n- and p-type dopants in the InSe monolayer via substitutional doping. *J Mater Sci* 52:7207–7214
36. Hu T, Zhou J, Dong JM (2017) Strain induced new phase and indirect-direct band gap transition of monolayer InSe. *Phys Chem Chem Phys* 19:21722–21728
37. Ahn Y, Shin M (2017) First-principles-based quantum transport simulations of monolayer indium selenide FETs in the ballistic limit. *IEEE Trans Electron Devices* 64(5):2129–2134
38. Fu ZM, Yang BW, Zhang N, Ma DW, Yang ZX (2018) First-principles study of adsorption-induced magnetic properties of InSe monolayers. *Appl Surf Sci* 436:419–423
39. Wagner P, Ivanovskaya VI, Franco MM, Humbert B, Adjizian JJ, Briddon PR, Ewels CP (2013) Stable hydrogenated graphene edge types: normal and reconstructed Klein edges. *Phys Rev B* 88:094106
40. Wang XF, Hu YB, Guo H (2012) Robustness of helical edge states in topological insulators. *Phys Rev B* 85:241402(R)
41. Wu TT, Wang XF, Zhai MX, Liu H, Zhou LP, Jiang YJ (2012) Negative differential spin conductance in doped zigzag graphene nanoribbons. *Appl Phys Lett* 100:052112
42. Datta S (2005) Quantum transport: atom to transistor. Cambridge University Press, New York
43. Ozaki T, Nishio K, Weng HM, Kino H (2010) Dual spin filter effect in a zigzag graphene nanoribbon. *Phys Rev B* 81:075422
44. Kan EJ, Li ZY, Yang JL, Hou JG (2007) Will zigzag graphene nanoribbon turn to half metal under electric field. *Appl Phys Lett* 91:243116
45. Xu B, Yin J, Xia YD, Wan XG, Jiang K, Liu ZG (2010) Electronic and magnetic properties of zigzag graphene nanoribbon with one edge saturated. *Appl Phys Lett* 96:163102
46. Nakabayashi J, Yamamoto D, Kurihara S (2009) Band-selective filter in a zigzag graphene nanoribbon. *Phys Rev Lett* 102:66803
47. Magda GZ, Jin XZ, Hagymasi I, Vancso P, Osváth Z, Nemes-Incze P, Hwang CY, Biro LP, Tapasztó L (2014) Room-temperature magnetic order on zigzag edges of narrow graphene nanoribbons. *Nature* 514:608

Submit your manuscript to a SpringerOpen[®] journal and benefit from:

- Convenient online submission
- Rigorous peer review
- Open access: articles freely available online
- High visibility within the field
- Retaining the copyright to your article

Submit your next manuscript at ► springeropen.com